PNAS RESEARCH ARTICLE | EARTH, ATMOSPHERIC, AND PLANETARY SCIENCES

Cambrian explosion condensed: High-precision geochronology of the lower Wood Canyon Formation, Nevada

Lyle L. Nelson[a,1], James L. Crowley[b], Emily F. Smith[c], Darin M. Schwartz[b], Eben B. Hodgin[d], and Mark D. Schmitz[b]

Edited by John Valley, University of Wisconsin-Madison, Madison, WI; received January 27, 2023; accepted May 25, 2023

The geologically rapid appearance of fossils of modern animal phyla within Cambrian strata is a defining characteristic of the history of life on Earth. However, temporal calibration of the base of the Cambrian Period remains uncertain within millions of years, which has resulted in mounting challenges to the concept of a discrete Cambrian explosion. We present precise zircon U–Pb dates for the lower Wood Canyon Formation, Nevada. These data demonstrate the base of the Cambrian Period, as defined by both ichnofossil biostratigraphy and carbon isotope chemostratigraphy, was younger than 533 Mya, at least 6 My later than currently recognized. This new geochronology condenses previous age models for the Nemakit–Daldynian (early Cambrian) and, integrated with global records, demonstrates an explosive tempo to the early radiation of modern animal phyla.

Ediacaran-Cambrian boundary | Cambrian explosion | U-Pb geochronology | geologic time scale | carbon isotope excursions

Significance

The early Cambrian Period marks the important interval when most major groups of animals first appear in Earth's sedimentary record. The tempo of this biological diversification is still poorly defined because, globally, there are few absolute age constraints that calibrate early Cambrian fossil occurrences or the carbon isotope perturbations used to correlate the biostratigraphy of different continents. In this study, we present high-precision age constraints for strata in the southwestern United States, which suggest the early Cambrian animal radiation was significantly faster than currently recognized. Accurately constraining the timing and rates of early animal evolution is a critical step toward better understanding this milestone in Earth's history.

The Ediacaran–Cambrian boundary marks the evolution and diversification of animals, manifested by the appearance of modern metazoan phyla in the fossil record. Initially proposed as a discrete epoch in the 1800s, the base of the Cambrian Period was considered to be a distinct break in the stratigraphic record between a diverse assemblage of trilobites and brachiopods and strata barren of any multicellular life and was marked by the first appearance of trilobites of the *Olenellus* Zone (1, 2). Yet, the subsequent recognition of late Precambrian macroscopic fossils well below the earliest trilobites (3), now known as Ediacaran biota (4), as well as a pretrilobitic skeletal fossil record, commonly termed "small shelly fossils" (5), muddied the definition. Formally, the base of the Cambrian is now defined by the first appearance of an ichnofossil assemblage that includes *Treptichnus pedum*, a distinctive branched, bilaterian trace fossil (6), interpreted as potentially formed by priapulids (7). The inclined branches of *T. pedum* are the earliest examples of systematic probing of the substrate, thus marking the onset of infaunalization that is pervasive in the Phanerozoic sedimentary record (8). In stratigraphic sections that lack abundant trace fossils, other secondary markers that have been adopted for recognizing the Ediacaran–Cambrian boundary include the disappearance of Ediacaran body fossils (9), the first appearance of certain small shelly fossils—a polyphyletic group of biomineralized body fossils (10), and a large negative carbon isotope excursion that has been termed the basal Cambrian carbon isotope excursion (BACE) (11). However, global correlations of these different markers—each with preservational limitations and based on observations of regional stratigraphic relationships—remain uncertain, particularly given the scarcity of radioisotopic dates within critical stratigraphic intervals of this age. In this contribution, we analyze detrital zircons with tandem laser ablation-inductively coupled plasma mass spectrometry (LA-ICPMS) and U–Pb isotope dilution-thermal ionization mass spectrometry (ID-TIMS) to establish new, precise maximum depositional ages (MDAs) for Ediacaran–Cambrian transition strata in the southern Great Basin and greatly revise age models for this eon-scale stratigraphic boundary.

Ediacaran–Cambrian Strata of the Southern Great Basin

The southern Great Basin of southeastern California and southern Nevada hosts well-exposed late Neoproterozoic and Cambrian strata deposited during rifting and ensuing passive margin development along the Cordilleran margin of Laurentia (Fig. 1). Although disturbed by Mesozoic–Cenozoic contractional, translational, and extensional deformation, regional stratigraphic architecture suggests a NW-facing continental margin during the late Ediacaran–early Cambrian (12, 13). In the southeastern Death Valley region, the lower member of the Wood Canyon Formation was deposited in shallow marine to deltaic environments proximal to the craton margin, while laterally equivalent strata of the Deep

Author contributions: L.L.N. and E.F.S. designed research; L.L.N., J.L.C., E.F.S., D.M.S., E.B.H., and M.D.S. performed research; and L.L.N. wrote the paper.

The authors declare no competing interest.

This article is a PNAS Direct Submission.

[1]To whom correspondence may be addressed. Email: lyle.nelson@carleton.ca.

This article contains supporting information online at https://www.pnas.org/lookup/suppl/doi:10.1073/pnas.2301478120/-/DCSupplemental.

Published July 17, 2023.

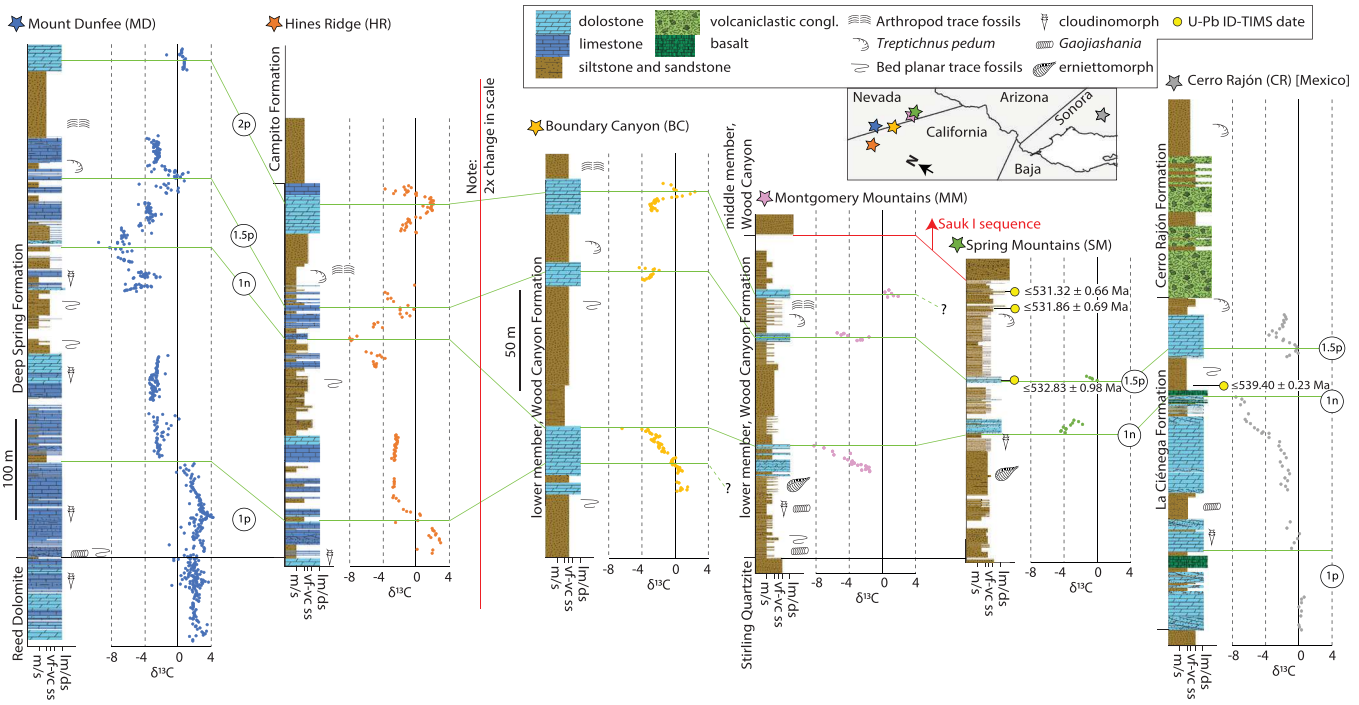

Fig. 1. Regional stratigraphic correlations of Ediacaran–Cambrian boundary strata in southwestern Laurentia. Stratigraphic, chemostratigraphic, and biostratigraphic data compiled from the following sources: MD—stratigraphy and chemostratigraphy (9), biostratigraphy (9, 14, 18); HR—stratigraphy and chemostratigraphy (13), biostratigraphy (13, 14); BC—stratigraphy and chemostratigraphy (13), biostratigraphy (19); MM—stratigraphy and chemostratigraphy (13, 20); biostratigraphy (13, 18, 20–22); SM—stratigraphy, chemostratigraphy, biostratigraphy, and geochronology (this study); CR—stratigraphy and biostratigraphy (23, 24), chemostratigraphy and geochronology (23). Carbon isotope data point colors and labeled carbon isotope excursions correspond to those in Fig. 4 composite chemostratigraphy. "1n" corresponds to the nadir of the BACE. Chemostratigraphic correlations are shown with green lines.

Spring Formation in the White and Inyo ranges (CA) and Esmeralda County (NV) thicken to the northwest and were deposited more distally to the margin (Fig. 1). Carbon isotope ($\delta^{13}C$) chemostratigraphy, biostratigraphy, and sequence stratigraphy have been used for correlation of these stratigraphic units across the basin (Fig. 1) (12–14). Southeast of Death Valley, in the Mojave Desert, fluvial-deltaic strata of the middle member of the Wood Canyon Formation onlap directly onto Proterozoic gneissic basement, marking the base of the Sauk megasequence that subsequently flooded the Laurentian craton (15–17).

In the Death Valley region, the lower member of the Wood Canyon Formation gradationally overlies quartz sandstone and pebble conglomerate of the Stirling Quartzite and consists primarily of siltstone to medium-grained sandstone deposited in shallow-marine to peritidal environments. The unit contains distinct dolostone marker units, that are characteristically coarsely recrystallized, but locally preserve primary fabrics that include ooids and stromatolites (13). Relatively expanded sections of the lower member in northwestern Death Valley (e.g., Boundary Canyon) preserve three dolostone marker units, while closer to the craton margin, two or no dolostone marker units are preserved, related to a combination of incision by the overlying middle member of the Wood Canyon and lateral facies transition to more proximal, deltaic environments (25). The lower part of the lower member of the Wood Canyon Formation, as well as the correlative Dunfee Member and lower Esmeralda Member of the Deep Spring Formation preserve Ediacaran-type body fossils including funnel-in-funnel biomineralized cloudinomorphs, annulated tubular fossils (c.f. *Gaojiashania*), and erniettomorphs (18, 20, 21, 26). Dolostone beds of the lower member of the Wood Canyon Formation and correlative carbonate units within the Deep Spring Formation preserve stratigraphically reproducible $\delta^{13}C$ values that preserve multiple negative and positive excursions, and the largest negative excursion (in the lowest dolostone marker unit of the lower Wood Canyon Formation and the Esmeralda Member of the Deep Spring Formation) is correlated to the BACE (13, 14, 19). The trace fossils *T. pedum*, *Rusophycus*, and *Monomorphicnus*, which are diagnostic of lower Cambrian strata, are preserved above the first positive excursion above the BACE (14, 19, 22). While no previous direct geochronology exists for the lower member of the Wood Canyon Formation, chemostratigraphic and biostratigraphic correlations to Sonora, Mexico suggest a MDA of 539.40 ± 0.23 Ma for the nadir of the BACE (23).

Geochronology, Biostratigraphy, and Chemostratigraphy of the Lower Member of the Wood Canyon Formation, Spring Mountains. Geochronology and carbonate chemostratigraphy samples were collected from a measured section of the lower member of the Wood Canyon Formation in the Spring Mountains, Nevada. Sample L2005-27.1 was collected from a <0.1 m micaceous siltstone bed within the second dolostone marker unit of the lower member of the Wood Canyon Formation. LA-ICPMS analyses yielded relatively large Mesoproterozoic peaks (c. 1.1 and 1.7 Ga), and smaller 1.4 Ga, Archean, and Ediacaran–Cambrian peaks. The five youngest ID-TIMS dates define a mode with a $^{206}Pb/^{238}U$ age of 532.83 ± 0.98/1.00/1.14 Ma [mean square weighted deviation (MSWD) = 0.8; probability of fit (pof) = 0.52] (Fig. 2). We conservatively interpret the MDA of the bed as the mode and SD of these dates, rather than the weighted mean, as this approach does not assume detrital or reworked grains are sampled from a population with a single-valued mean. Two older dates are 534.83 ± 1.15 Ma and 538.62 ± 0.69 Ma and are not included in the MDA calculations.

Sample L1906 was collected from a lenticular and discontinuous <0.2 m bed of siliceous micaceous green mudstone to siltstone preserved in between beds of coarse sandstone to pebble conglomerate within the upper part of the lower member of the Wood

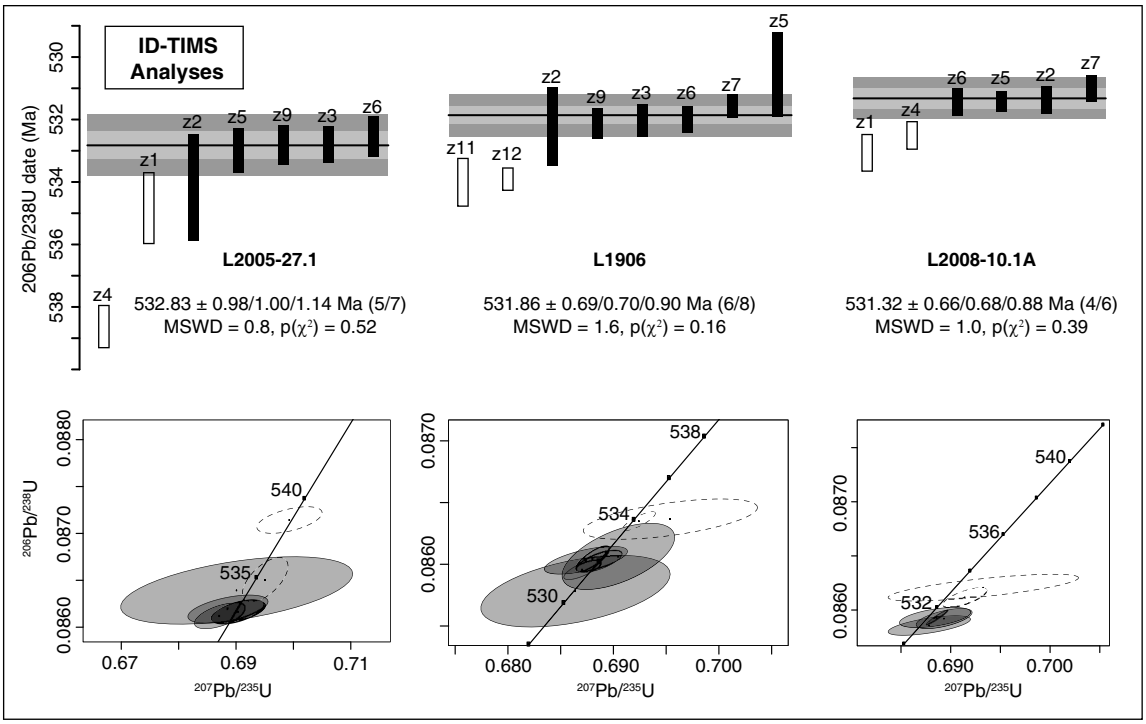

Fig. 2. U–Pb zircon geochronology of lower member of the Wood Canyon Formation. In ID-TIMS date distribution plots, analysis numbers (z#) correspond to Dataset S2. Vertical bars for $^{206}Pb/^{238}U$ dates represent 2*s* internal uncertainty of individual zircon analyses. Light horizontal gray bands represent the 95% CIs of the weighted mean dates, and dark horizontal gray bands represent the SDs of the mode of the youngest $^{206}Pb/^{238}U$ dates. Reported modes of the youngest $^{206}Pb/^{238}U$ dates include internal/internal and tracer/internal, tracer, and decay constant 95% CI uncertainties. ID-TIMS—isotope dilution–thermal ionization mass spectrometry; MSWD—mean square weighted deviation; p(χ2)—probability of fit.

Canyon Formation at the base of an interval dominated by peritidal to shallow marine quartz sandstone that directly underlies fluvial facies of the middle member. LA-ICPMS yielded a large c. 1.1 Ga peak, smaller 1.4 Ga and 1.7 Ga peaks, and a prominent Cambrian peak. The six youngest ID-TIMS dates have a mode at a $^{206}Pb/^{238}U$ age of 531.86 ± 0.69/0.70/0.90 Ma (MSWD = 1.6; pof = 0.16), interpreted as the MDA (Fig. 2). Two older dates are 533.91 ± 0.36 Ma and 534.01 ± 0.78 Ma.

Sample L2008-10.1A was collected from micaceous pale green siliceous siltstone ~9 m above L1906 and ~6 m below the base of the middle member of the Wood Canyon Formation. LA-ICPMS yielded similar populations to L1906. The four youngest ID-TIMS dates yield a mode at a $^{206}Pb/^{238}U$ age of 531.32 ± 0.66/0.68/0.88 Ma (MSWD = 1.0; pof = 0.39), interpreted as the MDA (Fig. 2). Two older dates are 532.51 ± 0.45 and 533.07 ± 0.60 Ma.

Pyrite-replaced cloudinomorphs with clear funnel-in-funnel structure are preserved within light green siltstone <5 m beneath the first dolostone marker unit (Fig. 3*A*). These are likely specimens of *Saarina hagadorni*, previously identified in the same taphonomic style within a correlative stratigraphic interval in the Montgomery Mountains (18, 20). One fossil cast of a partially preserved erniettomorph was found in sandstone ~20 m below the first dolostone marker unit, identified based on the preservation of sub-parallel ridges that are attributed to the sand-filled tubes diagnostic of erniettomorph walls (Fig. 3*B*). Abundant trace fossils, including *T. pedum*, identified based on the preservation of systematic oblique, inclined branches, are preserved on sandstone bed soles and top surfaces starting ~25 m above the second dolostone marker unit (Fig. 3 *C* and *D*).

Carbonate carbon isotope values ($\delta^{13}C$) in the lowest dolostone marker unit steadily increase from < –4‰ at the base to ~ –2‰, interpreted as part of the recovery from the nadir of the BACE (1n in Figs. 1 and 4*A*), based on regional stratigraphic and chemostratigraphic correlations. Within sections of the lower member of the Wood Canyon Formation more distal to the continental margin (e.g., Boundary Canyon and Montgomery Mountains), the lowest dolostone marker unit preserves the declining limb of the BACE, rather than the recovery (Fig. 1). This variability is interpreted to reflect slightly diachronous deposition of the dolostone units related to lateral migration of carbonate deposition, with Boundary Canyon recording the initial decline from positive $\delta^{13}C$ values to –4‰, Montgomery Mountains recording decline from –2‰ to the nadir of the excursion, and the Spring Mountains recording the subsequent rise in $\delta^{13}C$ values. This apparent diachroneity supports the interpretation of the $\delta^{13}C$ values as reflections of time-series changes in the carbon isotope composition of marine dissolved inorganic carbon. Carbon isotope values of the second dolostone marker unit in the Spring Mountains decrease from ~0‰ to < –2‰, interpreted as the downturn from the first positive excursion above the BACE (1.5p in Figs. 1, 4, and 5), again, based on regional correlations to more carbonate-rich sections. Although we acknowledge remaining uncertainty due to the fragmentary nature of the chemostratigraphic record of the siliciclastic-dominated Spring Mountains section, these suggested correlations are consistent with the lithostratigraphy and biostratigraphy (e.g., occurrences of pyritized cloudinomorphs and *T. pedum*).

Ediacaran–Cambrian Correlations in Southwest Laurentia. Sequence stratigraphy and carbon isotope chemostratigraphy across the southern Great Basin of California and Nevada are used to correlate Ediacaran–Cambrian transition units from more expanded sections in the White and Inyo ranges and Esmeralda County to more condensed sections in the Death Valley region, proximal to the craton margin (Fig. 1). Broadly, the upper Reed

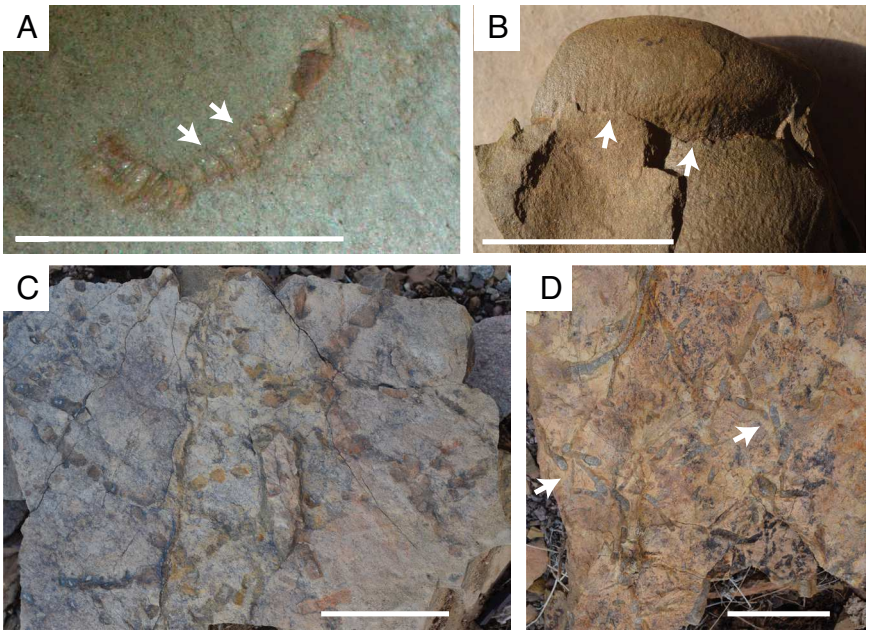

Fig. 3. Fossils in lower member of the Wood Canyon Formation, Spring Mountains. (*A*) Mold of pyritized cloudinomorph with characteristic tapered funnel-in-funnel structure preserved in siltstone ~3 m below first dolostone marker unit; arrows indicate pyritized funnel rims. (*B*) Cast of erniettomorph preserved in sandstone ~20 m beneath first dolostone marker unit with characteristic subparallel ridges (indicated with arrows) attributed to sand-filled tubes diagnostic of erniettomorph walls. (*C* and *D*) Examples of *T. pedum* on sandstone bed top (*C*) and sole (*D*) ~30 m above second dolostone marker unit, preserving oblique, inclined branches, indicated with arrows in (*D*). (Scale bar is 1 mm in *A* and 5 cm in *B*–*D*.)

Dolomite correlates to the upper Stirling Quartzite, the three members of the Deep Spring Formation correlate to the three dolostone capped sequences of the lower member of the Wood Canyon Formation, and the Campito Formation correlates to the middle member of the Wood Canyon Formation (12–14). More refined correlations can be drawn based on negative and positive $\delta^{13}C$ excursions: In Fig. 1, the nadir of the BACE is assigned to 1n, while 3 positive excursions are assigned (1p, 1.5p, 2p) to align with previously established nomenclature for basal Cambrian $\delta^{13}C$ chemostratigraphy (10). A composite $\delta^{13}C$ chemostratigraphic framework for the Ediacaran–Cambrian transition in southwest Laurentia is built using these correlations (Fig. 4*A*), and fossil occurrences are placed within this framework under the assumption that there is synchroneity in $\delta^{13}C$ trends across the basin.

It is important to acknowledge that local variability in early diagenesis can affect $\delta^{13}C$ trends (e.g., ref. 38), and further work remains to constrain potential impacts of diagenesis on Ediacaran–Cambrian carbonates of this specific basin. However, the hypothesis that their $\delta^{13}C$ values primarily reflect secular variations in marine composition rather than diagenesis is supported by the following observations: 1) Major excursions are regionally reproducible across significant lateral gradients in facies and environment spanning >250 km; 2) section-to-section variability in trends are consistent with depositional diachroneity of carbonate units (such as lateral differences observed within the first dolostone marker unit of the lower member of the Wood Canyon Formation); 3) continuity of excursions across major sequence boundaries suggests changes in relative sea level were not a major control on the trends; 4) lack of covariation among $\delta^{13}C$ and $\delta^{18}O$ values suggests meteoric diagenesis did not alter these isotopic compositions; and 5) lateral variability in dolomitization does not correspond to variability in preserved $\delta^{13}C$ trends (13).

Using this carbon isotope chemostratigraphic framework, the stratigraphically lowest MDA published here (sample L2005-27.1) establishes the 1.5p $\delta^{13}C$ excursion as ≤532.83 ± 0.98 Ma (Figs. 1, 2, and 4). The lowest occurrences of the trace fossils *T. pedum*, *Rusophycus*, and *Monomorphicnus* in multiple sections across the southern Great Basin are above the 1.5p excursion (Figs. 1, 3, and 4) (14, 19, 21, 23), and furthermore, the lowest identified occurrences of *T. pedum* in the Spring Mountains are ~25 m above sample L2005-27.1. Consequently, the lowest identified occurrences of trace fossils of both the *T. pedum* and *Rusophycus avalonensis* zones in the southern Great Basin are <532.83 ± 0.98 Ma. While the fossil record is inherently incomplete and the taphonomy of *T. pedum* is facies dependent (39), similar siliciclastic-dominated shallow-marine facies exist stratigraphically lower within the Wood Canyon and Deep Spring formations. Although it is possible that *T. pedum* could in fact predate this new MDA, until it is demonstrated to occur below this horizon, this is the best age constraint on the first appearance of this basal Cambrian index fossil within the southern Great Basin.

Global Calibration of the Ediacaran–Cambrian Boundary. Globally compiled U–Pb zircon age constraints on the first appearance of *T. pedum* demonstrate the ≤532.83 ± 0.98 date from the lower member of the Wood Canyon Formation is the best current constraint on the first appearance datum (FAD) of this index fossil (Fig. 4*B*). Although it is an MDA, dates above the *T. pedum* ichnofossil zone in Avalonia are within 2 My (31, 32), suggesting that this date approaches the true FAD (Fig. 4*B*). In Nova Scotia, the lower MacCodrum Brook Formation has a chemical abrasion ID-TIMS U–Pb zircon MDA of 531.86 ± 0.34 Ma (32), and in New Brunswick, the lower Ratcliffe Brook Formation has an ash bed air abrasion ID-TIMS date of 530.7 ± 0.9 Ma (31). Based on trace fossil and microfossil biostratigraphy, both of these correlate to the *R. avalonensis* zone of the Chapel Hill Formation in Newfoundland, which overlies the *T. pedum* zone (6).

Other sediment-bulldozing, unequivocally bilaterian trace fossils, such as treptichnids and *Parapsammichnites*, appear millions of years earlier, between c. 540 and 539 Ma, in the Nama Group of Namibia and South Africa (27, 40–42), as well as ~500 m below the Ediacaran–Cambrian boundary in the Dunfee Member of the Deep Spring Formation in Nevada (43). Previously, dates of c. 539 Ma from the upper Nama Group (34) were used to calibrate the Ediacaran–Cambrian boundary on the Geologic Time Scale (33). However, this calibration is problematic because 1) these units contain Ediacaran body fossils (27, 44) and 2) within this succession, the lowest stratigraphic occurrence of the ichnotaxon *T. pedum* (39) is above a major erosional sequence

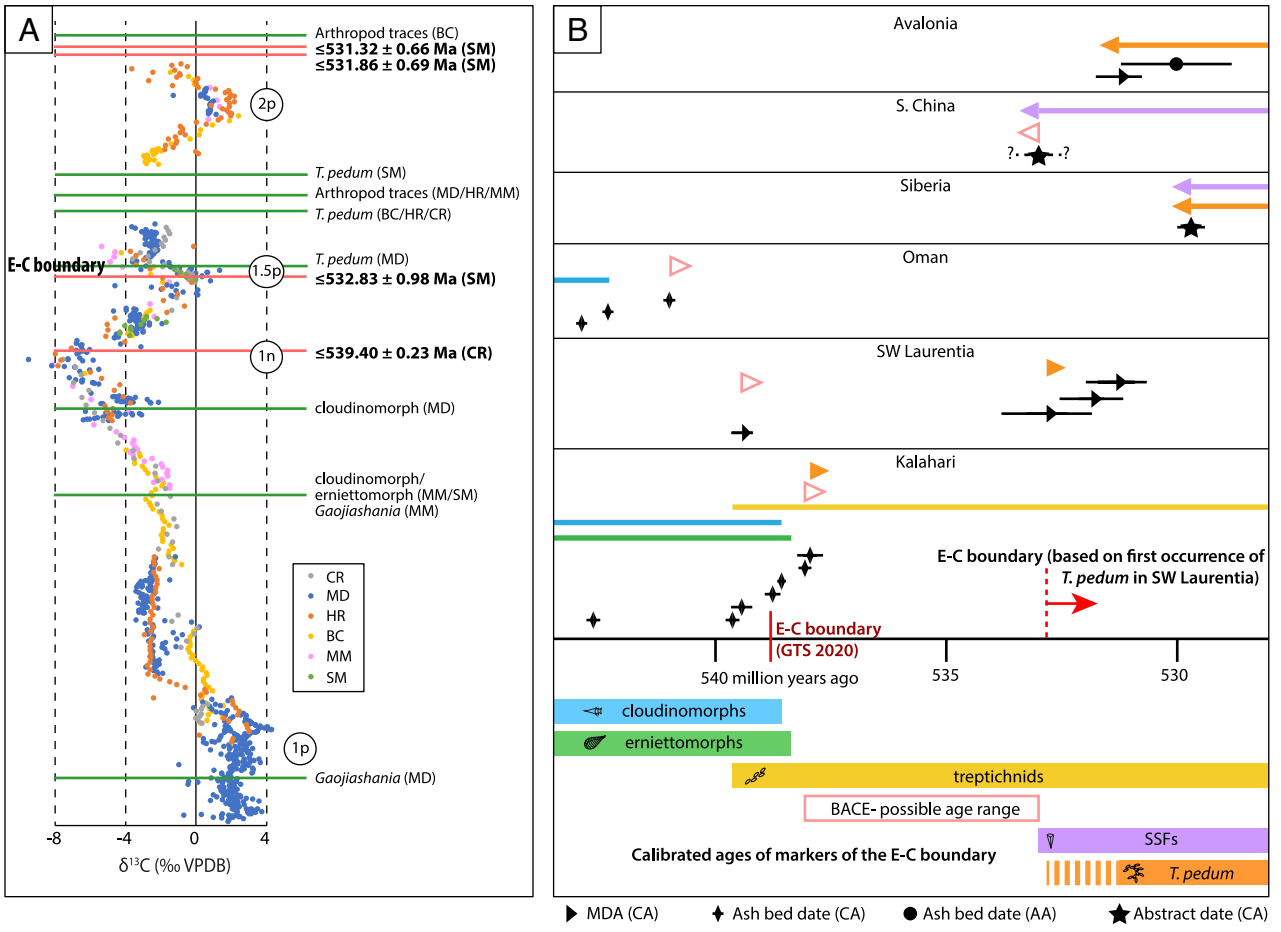

Fig. 4. (*A*) Composite carbon isotope chemostratigraphy of the Ediacaran–Cambrian boundary in southwestern Laurentia. Carbon isotope data are vertically scaled to the Mount Dunfee record using peaks for correlation; fossil occurrences and geochronology shown relative to chemostratigraphic framework. Data correspond to Fig. 1. CR—Cerro Rajón; MD—Mount Dunfee; HR—Hines Ridge; BC—Boundary Canyon; MM—Montgomery Mountains; SM—Spring Mountains; VPDB—Vienna Peedee Belemnite; p—positive excursion; n—negative excursion. (*B*) Globally compiled U–Pb ID-TIMS zircon geochronology of markers of the Ediacaran–Cambrian boundary. Colored arrows indicate stratigraphic position of markers relative to dated horizons (black symbols); colors correspond to markers indicated in lower part of figure. Geochronology data sources: Kalahari—(27); SW Laurentia—(ref. 23, this study); Oman—(28); Siberia—(29); S. China—(30); Avalonia—(31, 32); E-C boundary GTS 2020—(33), based on ref. 34. MDA—maximum depositional age; CA—chemical abrasion; AA—air abrasion; GTS—Geologic Time Scale; BACE—basal Cambrian carbon isotope excursion; SSFs—small shelly fossils; E-C—Ediacaran–Cambrian.

boundary that overlies all of the dated ash beds, and so is only constrained as <537.95 ± 0.28 Ma (27). Therefore, based on the integrated biostratigraphy and geochronology of southwestern Laurentia, the Ediacaran–Cambrian boundary, as it is currently defined by the first appearance of *T. pedum*, should now be recognized as ≤532.83 ± 0.98 Ma (Fig. 4*B*). Owing to the potential for regional biases in the preservation of trace fossil records, this proposed age could require revision if this index fossil assemblage is demonstrated to occur at an older stratigraphic horizon globally in the future.

The $\delta^{13}C$ record in southwestern Laurentia can be compared to early Cambrian chemostratigraphic records from other paleocontinents such as Morocco, Siberia, Mongolia, and South China (Fig. 5) (10). Recent isotopic studies of carbonate mud in the Bahamas lend credence to the fidelity of bulk micrite in tracking global marine carbon isotope compositions (45). While future work is imperative to continue probing the veracity of global carbonate carbon isotope correlations and the origin of these perturbations, evident similarities between records on disparate paleo-continents suggest that prevailing chemostratigraphic methods remain a useful framework for establishing global age models (e.g., ref. 10). Allowing the underlying assumptions of this convention, in southwest Laurentian $\delta^{13}C$ chemostratigraphic compilations, the 1p excursion correlates to the late Ediacaran positive isotope anomaly from global compilations (1p of ref. 10), 1n correlates to the nadir of the BACE, 1.5p is the positive excursion between 1p and 2p, and the subsequent positive excursion correlates to the 2p peak (Figs. 4 and 5).

Previous calibration of the Nemakit–Daldynian (early Cambrian) chemostratigraphic age model (10) relied on a 541.0 ± 0.13 Ma ash bed chemical abrasion ID-TIMS date at the base of the A4 carbonate stringer in Oman, which preserves a negative $\delta^{13}C$ excursion correlated to 1n (28). However, this constraint conflicts with recent data from successions in Mexico and South Africa, which suggest that 1n is ≤539.40 ± 0.23 Ma (23) and <538.04 ± 0.14 Ma (27), respectively. The discrepancy may be explained by the fact that the ash bed in Oman is at the base of a transgressive surface, associated with a lag in which underlying evaporites were dissolved and reworked (46), and thus could reasonably predate the preserved excursion. Taking these new inferences into account, the calibration of 1.5p to ≤532.83 ± 0.98 Ma demonstrates that the duration of the Nemakit–Daldynian (early Cambrian) is less than half that used in previously published age models—less than c. 8 m.y., rather than c. 16 m.y. (Fig. 5).

This recalibration of the $\delta^{13}C$ record can be applied to early Cambrian biostratigraphic records of SSF occurrences, which have been compiled from Siberia, Mongolia, and South China and placed within the context of the chemostratigraphic framework (10, 35). In Fig. 5, binned first occurrences of SSF genera from Siberia and

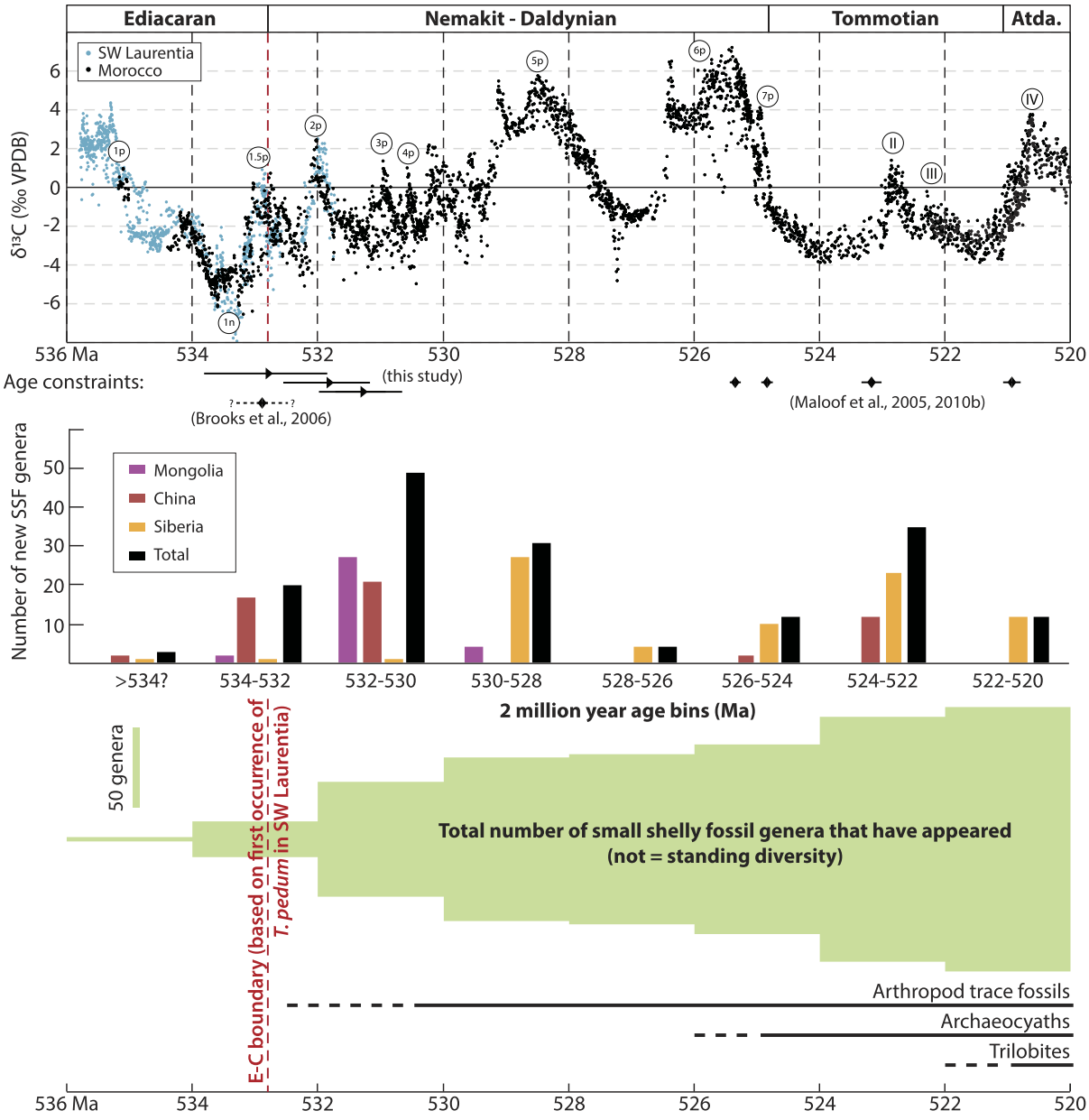

Fig. 5. Calibrated chemostratigraphy and biostratigraphy of the early Cambrian. Carbon isotope chemostratigraphy from southwestern Laurentia (this study) and Morocco (10), recalibrated using the MDA for 1.5p. Small shelly fossil (SSF) occurrences compiled by refs. 10 and 35 and recalibrated using the new chemostratigraphic age model. The terminal Nemakit–Daldynian and Tommotian age model is pinned by geochronology from refs. 36 and 37. In China, the lower Nemakit–Daldynian SSF occurrences are poorly constrained by chemostratigraphy but are constrained by a c. 533 Ma ash bed (30). In this compilation, fossil occurrences below this bed are binned to 534–532 Ma, and fossil occurrences above this bed are binned to 532 to 530 Ma. Arthropod trace fossil range from this study and ref. 32; archaeocyath fossil range from refs. 10 and 35; trilobite fossil range from ref. 10.

Mongolia are revised from ref. 10 using the updated $\delta^{13}C$ record calibration. In China, lower Nemakit–Daldynian SSF occurrences are poorly constrained by $\delta^{13}C$ chemostratigraphy but are constrained by a c. 533 Ma ash bed in the Meishucun section (30). In this compilation, fossil occurrences below this bed are binned into the 534 to 532-Ma window, and fossil occurrences above this bed are binned into the 532 to 530-Ma window. With the condensation of the Nemakit–Daldynian, most SSF occurrences previously suggested to be c. 540 to 533 Ma are <533 Ma. The resulting recalibration of SSF biostratigraphy indicates rates of animal diversification in the early Cambrian were at least twice as rapid as previously inferred.

The concept of the Cambrian explosion of animals has been challenged on the basis that is difficult to temporally define and instead suggested to be a series of transitional radiations over a protracted interval (e.g., ref. 47). In contrast, by compressing the age model for the polyphyletic SSF radiation approximately twofold, our results help to define a discrete interval of metazoan radiation leading up to the high levels of morphological disparity of iconic Cambrian fauna within Series 2 (48). In 1998, Stephen Jay Gould wrote: "The Cambrian explosion ranks as such a definitive episode in the history of animals that we cannot possibly grasp the basic tale of our own kingdom until we achieve better resolution for both the antecedents and the unfolding of this cardinal geological moment" (49). Improved radioisotopic age constraints are steadily enhancing the stratigraphic resolution of evolutionary and geochemical changes across the Ediacaran–Cambrian boundary. Over the last four decades, calibration of the base of the Cambrian Period has shifted progressively younger, from c. 570 Ma (50) to c. 544 Ma (51), to c. 541 Ma (28, 44), to c. 539 Ma (23, 34), and now to c. 533 Ma.

While paleontological studies reveal an increasingly apparent Ediacaran root to animal evolution (e.g., ref. 52), this revision to the geologic time scale lengthens the fuse and demonstrates that the early Cambrian radiation of modern animal phyla was even more explosive than formerly realized.

Materials and Methods

Three pale green, micaceous siliceous siltstone samples were collected from stratigraphic sections of the lower member of the Wood Canyon Formation measured north of Santa Cruz Spring in the Spring Mountains, Nevada (Fig. 1). At Boise State University, zircon grains were analyzed by LA-ICPMS, and grains yielding Ediacaran–Cambrian dates were dated by chemical abrasion ID-TIMS (see details in *SI Appendix*). The mode of the $^{206}Pb/^{238}U$ dates from the youngest population is interpreted as the MDA of the sampled bed and reported at 95% CI in the format ± *X*/*Y*/*Z* Ma (Fig. 2), where *X* is the internal error based on analytical uncertainties only, *Y* includes *X* and the tracer calibration uncertainty, and *Z* includes *Y* and the ^{238}U decay constant uncertainty (53).

Carbonate samples collected from dolostone beds of the lower member of the Wood Canyon Formation were microdrilled for powder along laminations and analyzed at the Johns Hopkins University Isotope Ratio Mass Spectrometer Laboratory for $\delta^{13}C$ and $\delta^{18}O$ isotopic compositions using a GasBench II peripheral device coupled to a Thermo-Finnigan MAT253 isotope ratio mass spectrometer in continuous-flow mode (see details in *SI Appendix*). Carbon and oxygen isotope ratios are reported in per mil notation relative to VPDB, and SD (1σ) of $\delta^{13}C$ and $\delta^{18}O$ values for in-house standards was <0.02‰ and <0.06‰, respectively.

Data, Materials, and Software Availability. All study data are included in the article and/or supporting information.

ACKNOWLEDGMENTS. Analytical work was supported by the AGeS2 program via support from NSF awards EAR-1759200 and -1759353, and by NSF EAR-2021064 and -2144836 to E.F.S. L.L.N. was supported in part by NSF Graduate Research Fellowship DGE-1746891. Any opinions, findings, and conclusions or recommendations expressed in this material are those of the authors and do not necessarily reflect the views of the NSF. We thank L. Webb, I. Bennett, and J. Ramezani for mineral separation assistance and D. Brenner and M. Lonsdale for stable isotope measurements. We thank H. Maddin and R. Gathaz for use of photomicrography equipment. We thank the Spring Mountains National Recreation Area for research access. We thank F. Macdonald for comments on an earlier draft. We are grateful to three anonymous reviewers for constructive suggestions that improved this manuscript.

Author affiliations: [a]Department of Earth Sciences, Carleton University, Ottawa, ON K1S 0V9, Canada; [b]Department of Geosciences, Boise State University, Boise, ID 83725; [c]Department of Earth and Planetary Sciences, Johns Hopkins University, Baltimore, MD 21218; and [d]Department of Earth, Environmental and Planetary Sciences, Brown University, Providence, RI 02912

1. C. D. Walcott, "The fauna of the Lower Cambrian or Olenellus Zone" in Tenth Annual Report of the Director, 1888-1889. Part 1 (United States Geological Survey, 1890), pp. 509–774.
2. H. E. Wheeler, Base of the Cambrian system. *J. Geol.* **55**, 153–159 (1947).
3. R. C. Sprigg, Early Cambrian (?) jellyfishes from the flinders ranges, South Australia. *Trans. R. Soc. S. Aust.* **71**, 212–224 (1947).
4. J. G. Gehling, Environmental interpretation and a sequence stratigraphic framework for the terminal Proterozoic Ediacara Member within the Rawnsley Quartzite, South Australia. *Precambrian Res.* **100**, 65–95 (2000).
5. S. T. Matthews, V. V. Missarzhevsky, Small shelly fossils of late Precambrian and early Cambrian age: A review of recent work. *J. Geol. Soc.* **131**, 289–303 (1975).
6. E. Landing, Precambrian-Cambrian boundary global stratotype ratified and a new perspective of Cambrian time. *Geology* **22**, 179–182 (1994).
7. J. Vannier, I. Calandra, C. Gaillard, A. Żylińska, Priapulid worms: Pioneer horizontal burrowers at the Precambrian-Cambrian boundary. *Geology* **38**, 711–714 (2010).
8. L. A. Buatois, *Treptichnus pedum* and the Ediacaran-Cambrian boundary: significance and caveats. *Geol. Mag.* **155**, 174–180 (2018).
9. E. F. Smith *et al.*, The end of the Ediacaran: Two new exceptionally preserved body fossil assemblages from Mount Dunfee, Nevada, USA. *Geology* **44**, 911–914 (2016).
10. A. C. Maloof *et al.*, The earliest Cambrian record of animals and ocean geochemical change. *GSA Bull.* **122**, 1731–1774 (2010).
11. M. Zhu *et al.*, Cambrian integrative stratigraphy and timescale of China. *Sci. China Earth Sci.* **62**, 25–60 (2019).
12. J. H. Stewart, "Upper Precambrian and Lower Cambrian strata in the southern Great Basin, California and Nevada" (U.S. Geological Survey Professional Paper 620, United States Government Printing Office, Washington, D.C., 1970), p. 206.
13. E. F. Smith, L. L. Nelson, N. O'Connell, A. Eyster, M. C. Lonsdale, The Ediacaran–Cambrian transition in the southern Great Basin, United States. *GSA Bull.* **135**, 1393–1414 (2022).
14. F. A. Corsetti, J. W. Hagadorn, The Precambrian-Cambrian transition in the southern Great Basin, USA. *Sediment. Record* **1**, 4–8 (2003).
15. L. L. Sloss, Sequences in the cratonic interior of North America. *Geol. Soc. Am. Bull.* **74**, 93–114 (1963).
16. C. M. Fedo, J. D. Cooper, Sedimentology and sequence stratigraphy of Neoproterozoic and Cambrian units across a craton-margin hinge zone, southeastern California, and implications for the early evolution of the Cordilleran margin. *Sediment. Geol.* **141**, 501–522 (2001).
17. M. Keller, J. D. Cooper, O. Lehnert, "Sauk megasequence supersequences, southern Great Basin: Second-order accommodation events on the southwestern Cordilleran margin platform" in *The Great American Carbonate Bank: The Geology and Economic Resources of the Cambrian–Ordovician Sauk Megasequence of Laurentia*, Derby J. R., Fritz R. D., Longacre S. A., Morgan W. A., Sternbach C. A., Eds. (AAPG Memoir, 2012), **vol. 98**, pp. 873–896.
18. T. Selly *et al.*, A new cloudinid fossil assemblage from the terminal Ediacaran of Nevada, USA. *J. Syst. Palaeontol.* **18**, 357–379 (2020).
19. F. A. Corsetti, J. W. Hagadorn, Precambrian-Cambrian transition: Death Valley, United States. *Geology* **28**, 299–302 (2000).
20. E. F. Smith, L. L. Nelson, S. M. Tweedt, H. Zeng, J. B. Workman, A cosmopolitan late Ediacaran biotic assemblage: New fossils from Nevada and Namibia support a global biostratigraphic link. *Proc. R. Soc. B Biol. Sci.* **284**, 20170934 (2017).
21. J. W. Hagadorn, B. Waggoner, Ediacaran fossils from the southwestern Great Basin, United States. *J. Paleontol.* **74**, 349–359 (2000).
22. S. Jensen, M. L. Droser, N. A. Heim, Trace fossils and ichnofabrics of the Lower Cambrian Wood Canyon Formation, southwest Death Valley area in *Proterozoic-Cambrian of the Great Basin and Beyond, SEPM Fieldtrip Guidebook*, Corsetti F. A., Ed. (Pacific Section of the SEPM, Fullerton, CA, 2002), pp. 123–135.
23. E. B. Hodgin *et al.*, A link between rift-related volcanism and end-Ediacaran extinction? Integrated chemostratigraphy, biostratigraphy, and U-Pb geochronology from Sonora, Mexico. *Geology* **49**, 115–119 (2021).
24. A. J. Barrón-Díaz, F. A. Paz-Moreno, J. W. Hagadorn, The Cerro Rajón Formation–A new lithostratigraphic unit proposed for a Cambrian (Terreneuvian) volcano-sedimentary succession from the Caborca region, northwest Mexico. *J. South Am. Earth Sci.* **89**, 197–210 (2019).
25. E. G. Hogan, C. M. Fedo, J. D. Cooper, Reassessment of the basal Sauk supersequence boundary across the Laurentian craton-margin hinge zone, southeastern California. *J. Geol.* **119**, 661–685 (2011).
26. R. Horodyski, Late Proterozoic megafossils from southern Nevada. *Geol. Soc. Am. Abstracts with Programs* **23**, 163 (1991).
27. L. L. Nelson *et al.*, Pushing the boundary: A calibrated Ediacaran-Cambrian stratigraphic record from the Nama Group in northwestern Republic of South Africa. *Earth Planet. Sci. Lett.* **580**, 117396 (2022).
28. S. A. Bowring *et al.*, Geochronologic constraints on the chronostratigraphic framework of the Neoproterozoic Huqf Supergroup, Sultanate of Oman. *Am. J. Sci.* **307**, 1097–1145 (2007).
29. A. J. Kaufman *et al.*, A shorter fuse for the Cambrian Explosion? *Geol. Soc. Am. Abstracts with Programs* **44**, 326 (2012).
30. B.-G.J. Brooks, J. L. Crowley, S. A. Bowring, C. Cervato, J. Yugan, A new U/Pb date for the basal Meishucun section and implications for the timing of the Cambrian explosion: *University of Sheffield, The Palaeontological Association, 50th Annual Meeting Abstracts*, 18 (2006).
31. C. E. Isachsen, S. A. Bowring, E. Landing, S. D. Samson, New constraint on the division of Cambrian time. *Geology* **22**, 496–498 (1994).
32. S. M. Barr *et al.*, The Terreneuvian MacCodrum Brook section, Mira terrane, Cape Breton Island, Nova Scotia, Canada: Age constraints from ash layers, organic-walled microfossils, and trace fossils. *Can. J. Earth Sci.* **60**, 307–332 (2022).
33. S. C. Peng, L. E. Babcock, P. Ahlberg, "The Cambrian Period" in *The Geologic Time Scale 2020*, F. M. Gradstein, J. G. Ogg, M. D. Schmitz, G. M. Ogg, Eds. (Elsevier, 2020), pp. 565–629.
34. U. Linnemann *et al.*, New high-resolution age data from the Ediacaran-Cambrian boundary indicate rapid, ecologically driven onset of the Cambrian explosion. *Terra Nova* **31**, 49–58 (2019).
35. E. F. Smith, F. A. Macdonald, T. A. Petach, U. Bold, D. P. Schrag, Integrated stratigraphic, geochemical, and paleontological late Ediacaran to early Cambrian records from southwestern Mongolia. *GSA Bull.* **128**, 442–468 (2016).
36. A. C. Maloof, D. P. Schrag, J. L. Crowley, S. A. Bowring, An expanded record of Early Cambrian carbon cycling from the Anti-Atlas Margin, Morocco. *Can. J. Earth Sci.* **42**, 2195–2216 (2005).
37. A. C. Maloof *et al.*, Constraints on early Cambrian carbon cycling from the duration of the Nemakit-Daldynian–Tommotian boundary $\delta^{13}C$ shift, Morocco. *Geology* **38**, 623–626 (2010).
38. J. A. Higgins *et al.*, Mineralogy, early marine diagenesis, and the chemistry of shallow-water carbonate sediments. *Geochim. Cosmochim. Acta* **220**, 512–534 (2018).
39. J. P. Wilson *et al.*, Deep-water incised valley deposits at the Ediacaran-Cambrian boundary in southern Namibia contain abundant *Treptichnus pedum*. *Palaios* **27**, 252–273 (2012).
40. S. Jensen, B. Z. Saylor, J. G. Gehling, G. J. Germs, Complex trace fossils from the terminal Proterozoic of Namibia. *Geology* **28**, 143–146 (2000).
41. L. A. Buatois, J. Almond, M. G. Mángano, S. Jensen, G. J. Germs, Sediment disturbance by Ediacaran bulldozers and the roots of the Cambrian explosion. *Sci. Rep.* **8**, 1–9 (2018).
42. S. A. Darroch *et al.*, The trace fossil record of the Nama Group, Namibia: Exploring the terminal Ediacaran roots of the Cambrian explosion. *Earth Sci. Rev.* **212**, 103435 (2021).
43. L. G. Tarhan, P. M. Myrow, E. F. Smith, L. L. Nelson, P. M. Sadler, Infaunal augurs of the Cambrian explosion: An Ediacaran trace fossil assemblage from Nevada, USA. *Geobiology* **18**, 486–496 (2020).
44. J. P. Grotzinger, S. A. Bowring, B. Z. Saylor, A. J. Kaufman, Biostratigraphic and geochronologic constraints on early animal evolution. *Science* **270**, 598–604 (1995).

45. E. C. Geyman *et al.*, The origin of carbonate mud and implications for global climate. *Proc. Natl. Acad. Sci. U.S.A.* **119**, 2210617119 (2022).
46. J. Grotzinger, Z. Al-Rawahi, Depositional facies and platform architecture of microbialite-dominated carbonate reservoirs, Ediacaran-Cambrian Ara Group, Sultanate of Oman. *AAPG Bull.* **98**, 1453–1494 (2014).
47. R. Wood *et al.*, Integrated records of environmental change and evolution challenge the Cambrian Explosion. *Nat. Ecol. Evol.* **3**, 528–538 (2019).
48. X. Hou, R. J. Aldridge, J. Bergström, D. J. Siveter, F. Xiang-Hong, *The Cambrian Fossils of Chengjiang, China: The Flowering of Early Animal Life* (Oxford, Blackwell Science, 2004), p. 233.
49. S. J. Gould, On embryos and ancestors. *Nat. Hist.* **107**, 58–65 (1998).
50. W. B. Harland *et al.*, *A Geologic Time Scale* (Cambridge University Press, 1982), vol. 1, p. 131.
51. S. A. Bowring *et al.*, Calibrating rates of Early Cambrian evolution. *Science* **261**, 1293–1298 (1993).
52. M. L. Droser, J. G. Gehling, The advent of animals: The view from the Ediacaran. *Proc. Natl. Acad. Sci. U.S.A.* **112**, 4865–4870 (2015).
53. A. H. Jaffey, K. F. Flynn, L. E. Glendenin, W. T. Bentley, A. M. Essling, Precision measurement of half-lives and specific activities of U 235 and U 238. *Phys. Rev. C* **4**, 1889 (1971).